International Information and Engineering Technology Association
Advancing the World of Information and Engineering

Revue des Composites et des Matériaux Avancés-Journal of Composite and Advanced Materials
Vol. 36, No. 4, August, 2026, pp. 823-831
Journal homepage: http://iieta.org/journals/rcma

Effect of Flux Particle Size and Binary Flux Mixtures on Weld Bead Geometry and Mechanical Properties in Submerged Arc Welding of Liquefied Petroleum Gas Cylinders: An Experimental Study

Khouloud Baali*, Salah Madani, Abdallah Bourih, Ahmed Boussaha, Youcef Djebara

Laboratory of Structural Mechanics and Materials, Department of Mechanical Engineering, Faculty of Technology, University of Batna 2-Mostefa Ben Boulaid, Batna 05000, Algeria

Corresponding Author Email: khouloud.baali@univ-batna2.dz

https://doi.org/10.18280/rcma.360411

Received: 12 June 2026
Revised: 10 August 2026
Accepted: 21 August 2026
Available online: 31 August 2026

Keywords:
flux particle size, Liquefied Petroleum Gas cylinders, mechanical properties, microhardness, submerged arc welding, tensile strength, weld bead geometry

ABSTRACT

Submerged arc welding (SAW) is widely used in industrial applications where high productivity and consistent weld quality are required. This experimental study investigates the effect of welding flux particle size distribution (PSD) on the weld bead geometry and mechanical properties of low-carbon steel joints commonly used in Liquefied Petroleum Gas (LPG) cylinder manufacturing. All welding parameters were kept constant to isolate the effect of flux PSD. Four flux particle size categories were examined: coarse (A), medium (B), fine (C), and very fine (D). In addition, binary flux mixtures were prepared by combining coarse flux A with very fine flux D in proportions ranging from 20% to 80%. The effects of these flux conditions on penetration depth, bead width, reinforcement height, and tensile properties were evaluated. The results show that flux PSD affects both weld geometry and mechanical properties. Intermediate mixtures containing approximately 50–60% fine particles produced favorable weld characteristics, including adequate penetration, reduced bead width, and stable reinforcement. These findings indicate that a balanced flux PSD is important for optimizing the overall quality and tensile performance of SAW joints.

1. INTRODUCTION

A Liquefied Petroleum Gas (LPG) cylinder is a type of pressure vessel used to store and transport liquefied gases. Therefore, the welds used in LPG cylinders must meet high requirements in terms of strength, leak-tightness, and metallurgical integrity [1-5]. Because of the efficiency and economic benefits of the submerged arc welding (SAW) process for long welds and thicker plates, as well as the high quality of the resulting welds, this process is commonly used in the manufacturing of LPG cylinders [6-8].

One of the principal factors influencing weld quality is the granular flux [9-16], which shields the molten pool, provides alloying components, stabilizes the arc, and influences the thermal conditions and the resulting microstructure. Many studies have examined flux chemistry and its effects on weld-metal chemistry and metallurgical behavior [17-21]. Other studies have investigated the effects of welding parameters on weld bead geometry and weld characteristics. However, compared with flux chemistry, fewer studies have specifically addressed the effect of flux particle size and particle size distribution (PSD) in SAW [22-26].

Flux particle size can affect the permeability of the flux bed, heat transfer to the molten metal, slag solidification behavior, and consequently weld bead geometry and mechanical properties. In particular, Garg et al. [23] investigated the influence of flux particle size and flux column height on weld bead geometry, demonstrating that flux PSD can significantly influence the welding response.

However, the available literature has primarily considered individual particle-size ranges or the general characteristics of commercial fluxes (CFs). The effect of deliberately combining distinct coarse and fine particle fractions to produce controlled binary PSD has received comparatively limited attention. In particular, the influence of systematic variations in the proportion of coarse and very fine flux particles on weld bead geometry and mechanical properties under identical welding conditions remains insufficiently documented.

To address this research gap, the present work investigates the influence of flux PSD on the weld bead geometry and mechanical properties of SAW welds intended for LPG cylinder fabrication. Four distinct base flux particle size categories were selected: coarse (A), medium (B), fine (C), and very fine (D). Binary mixtures were prepared by blending flux A with flux D at proportions ranging from 20 to 80 wt.% D to evaluate the combined effects of coarse and fine particle fractions. All welding conditions were kept constant to isolate the effect of flux PSD. The objective of this study is to evaluate the relationship between flux PSD and key performance indicators, including weld bead geometry, tensile properties, and microhardness distribution.

2. EXPERIMENTAL PROCEDURE

2.1 Materials and flux preparation

In this experimental investigation, a commercial steel plate with a thickness of 3 mm was used as the workpiece material. The base material was ASTM A36 low-carbon steel [27], which is commonly used in welded applications. Its chemical composition is presented in Table 1. The sheets were cut into specimens suitable for welding and subsequent mechanical characterization.

The filler wire conformed to the ASME SFA-5.17 classification [28], and its chemical composition is presented in Table 2. The commercial SAW flux (CF), classified as SA AR 1 77 AC according to ISO 14174 [29], was supplied by the manufacturer with a nominal particle size range of 0.2–2 mm. Its chemical composition is presented in Table 3.

Table 1. Chemical composition of the base material

Content of Chemical Elements (wt.%)								
C	Si	Mn	P	S	Cr	Al	Cu	Ni
0.2	0.00	0.77	0.01	0.05	0.02	0.03	0.01	0.00
0	79	8	56	8	1	5	2	75

Table 2. Chemical composition of the filler wire

Content of Chemical Elements (wt.%)					
C	Si	Mn	P	S	Cu
0.04-0.14	≤0.10	0.25-0.60	≤0.030	≤0.030	≤0.35

Table 3. Chemical composition of the commercial submerged arc welding (SAW) flux

Content of Chemical Elements (wt.%)		
$SiO_2 + TiO_2$	$Al_2O_3 + MnO$	$CaF_2 + CaO + MgO$
25	55	15

However, the manufacturer did not provide a detailed quantitative PSD. In this study, no additional quantitative PSD analysis, such as sieve-based mass fraction measurements, was performed on the as-supplied CF. Therefore, the relative proportions of the different particle size fractions within CF were not determined. For the preparation of the experimental flux grades, CF was separated using five standard sieves into four nominal particle size classes (Figure 1).

Figure 1. Set of standard sieves used for grading the flux

Based on the sieve analysis, four nominal grain size ranges were used: A (coarse), 1.0–2.0 mm; B (medium), 0.5–1.0 mm; C (fine), 0.25–0.5 mm; and D (very fine), 0.15–0.25 mm. Figure 2 shows close-up images of the different flux grades used in the study.

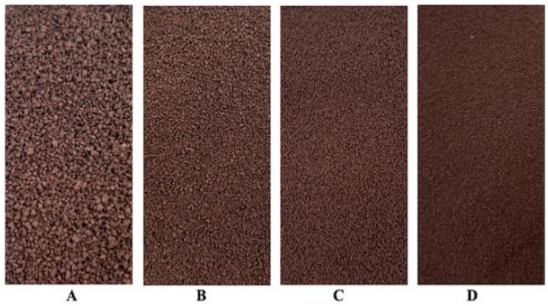

Figure 2. Four grades of flux used in the study

Binary mixtures of A and D were also prepared with D fractions of 20, 30, 40, 50, 60, 70, and 80 wt.% and tested. The mixtures were designated AD20, AD30, AD40, AD50, AD60, AD70, and AD80, respectively.

The aim of this series was to examine how the partial addition of very fine particles affects slag coverage, arc stability, and bead uniformity while maintaining some of the penetration characteristics of the coarse flux.

2.2 Welding procedure

All welds were performed using a constant, automated SAW setup to ensure consistency. The welding parameters were kept constant for all experiments: current = 248 A, voltage = 26.5 V, and travel speed = 420 mm/min. Accordingly, the heat input remained constant and was not considered an independent variable. The observed variations in penetration and bead geometry were mainly attributed to flux PSD and its effect on heat transfer. The welding operation is shown in Figure 3, and examples of the welded samples are shown in Figure 4.

Figure 3. Welding operation

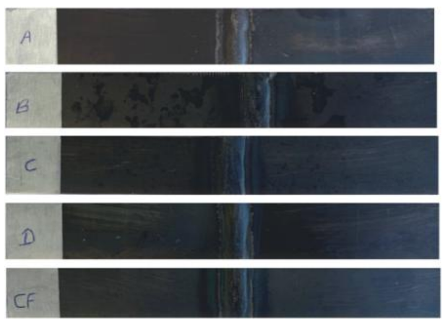

Figure 4. Samples welded using submerged arc welding (SAW) with different flux grades

2.3 Characterization techniques

2.3.1 Weld bead geometry

Cross-sections of the welded joints were prepared using standard metallographic procedures and examined after polishing. The bead width (W), penetration depth (P), and reinforcement height (H) were measured from images of the polished cross-sections. Three independent welded specimens were prepared for each flux condition. For each specimen, three measurements were taken for each bead geometry parameter and averaged to obtain a single specimen-level value. The mean and standard deviation (SD) for each flux condition were then calculated from the three specimen-level values (n = 3). Thus, the statistical analysis was based on three independent specimens per flux condition, rather than on the nine individual measurements.

2.3.2 Tensile testing

Transverse tensile specimens were machined from the welded joints according to the relevant testing requirements. Three tensile specimens were tested for each flux condition in accordance with ASTM A370 [30]. Ultimate tensile strength (UTS), yield strength (YS), and elongation were determined for each specimen. The reported tensile properties for each flux condition are presented as mean ± SD, calculated from the three independent specimens (n = 3). YS was determined using the 0.2% offset method. The stress–strain curves presented in Section 3.3 are based on engineering stress and engineering strain.

2.3.3 Microhardness testing

Vickers microhardness measurements were performed across the weld cross-section, including the weld metal (WM), heat-affected zone (HAZ), and base metal (BM), for each flux condition according to EN ISO 9015-2 [31]. A load of 1 kg was applied for 15 s at a constant laboratory temperature of 22 °C.

3. RESULTS AND DISCUSSION

3.1 Weld bead geometry

Weld bead geometry has a significant influence on weld quality in SAW [32, 33]. The main bead geometry parameters are illustrated in Figure 5, while representative macrographs of the polished weld cross-sections used for bead geometry analysis are presented in Figure 6.

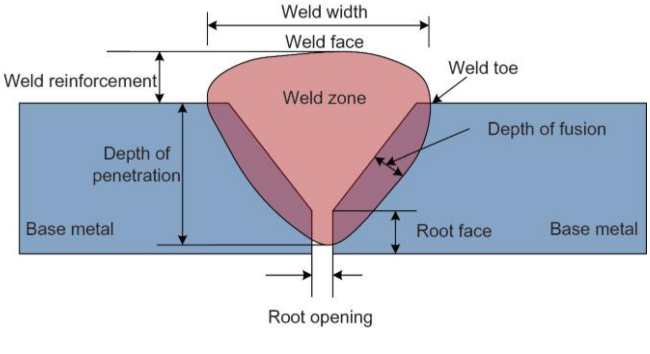

Figure 5. Major elements of the weld bead geometry

The effects of flux particle size on various weld bead geometry parameters are summarized in the graphs and tables below. First, the effect of flux particle size on weld bead geometry was investigated using CF and four flux grades with average particle sizes of A (1.5 mm), B (0.75mm), C (0.375 mm), and D (0.2 mm), as shown in Figure 7 and Table 4.

As shown in Figure 7, although the trends are not strictly linear, the weld bead geometry is significantly affected by the flux particle size. Compared with CF, the use of fluxes A, B, C, and D resulted in an increase in both bead width and penetration depth, with the largest increase in bead width observed for flux B and the greatest increase in penetration depth observed for flux D. However, the reinforcement height was slightly reduced, with the most noticeable reduction observed for flux D.

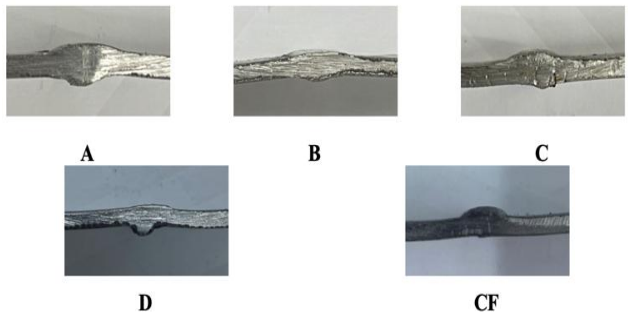

Figure 6. Macrographs of polished weld cross-sections for the different flux grades: Coarse (A), medium (B), fine (C), very fine (D) and commercial flux (CF)

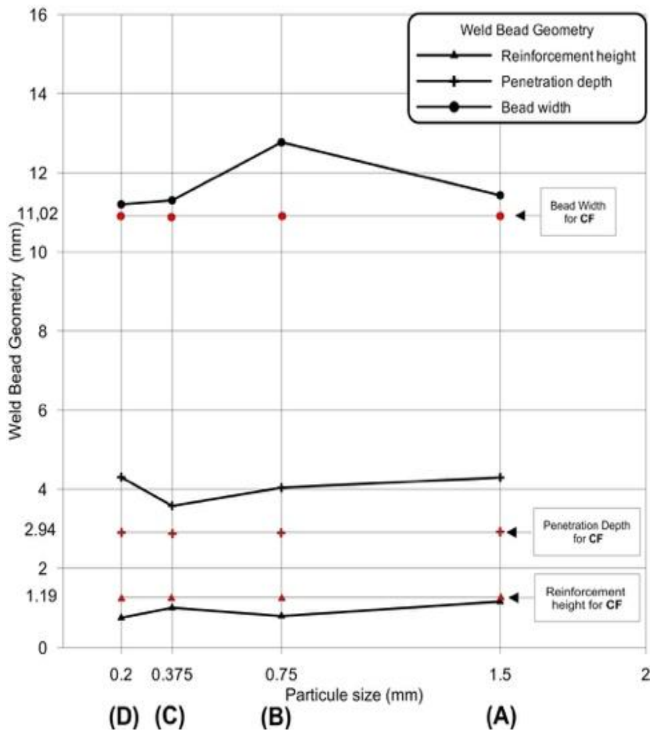

Figure 7. Effect of flux particle size on weld bead geometry parameters for A, B, C, D, and CF

Note: Values are mean ± SD (n = 3). Coarse (A), medium (B), fine (C), very fine (D) and commercial flux (CF). The commercial flux (CF) was tested as supplied (with its original particle size distribution), while fluxes A–D were obtained by sieving the same base flux into distinct particle size fractions.

The effect of combining flux A with flux D at different D fractions, ranging from 20 to 80% in 10% increments, is presented in Figure 8 and Table 5. The results show that the weld bead geometry was affected by the PSD of the SAW flux. Noticeable changes were observed, particularly in bead width and penetration depth, as the proportion of fine-grained flux D increased in the coarse-grained flux A.

Table 4. Weld bead geometry parameters for CF and flux grades A–D (mean ± standard deviation, n = 3)

Flux	Particle Size, mm	Reinforcement Height (H), mm	Penetration Depth (P), mm	Bead Width (W), mm
A	1.5	1.16 ± 0.1	4.3 ± 0.1	11.43 ± 0.06
B	0.75	0.795 ± 0.07	4.04 ± 0.23	12.77 ± 1.44
C	0.375	1.005 ± 0.02	3.58 ± 0.03	11.305 ± 0.93
D	0.2	0.753 ± 0.02	4.303 ± 0.31	11.203 ± 0.28
CF	As supplied	1.19 ± 0.04	2.94 ± 0.14	11.02 ± 0.06

Note: The commercial flux (CF) was tested as supplied (with its original particle size distribution), while fluxes A–D were obtained by sieving the same base flux into distinct particle size fractions.

Table 5. Weld bead geometry parameters for A–D flux mixtures (mean ± standard deviation, n = 3)

D Fraction in A, wt.%	Reinforcement Height (H), mm	Penetration Depth (P), mm	Bead Width (W), mm
20	1.005 ± 0.02	5.125 ± 0.04	10.235 ± 0.05
30	0.966 ± 0.04	4.303 ± 0.11	10.691 ± 0.34
40	0.951 ± 0.03	4.203 ± 0.16	10.653 ± 0.21
50	0.955 ± 0.05	4.270 ± 0.20	9.415 ± 0.05
60	0.932 ± 0.10	4.573 ± 0.32	9.512 ± 0.62
70	1.033 ± 0.02	4.632 ± 0.26	9.816 ± 0.16
80	1.022 ± 0.07	4.488 ± 0.35	10.585 ± 0.32

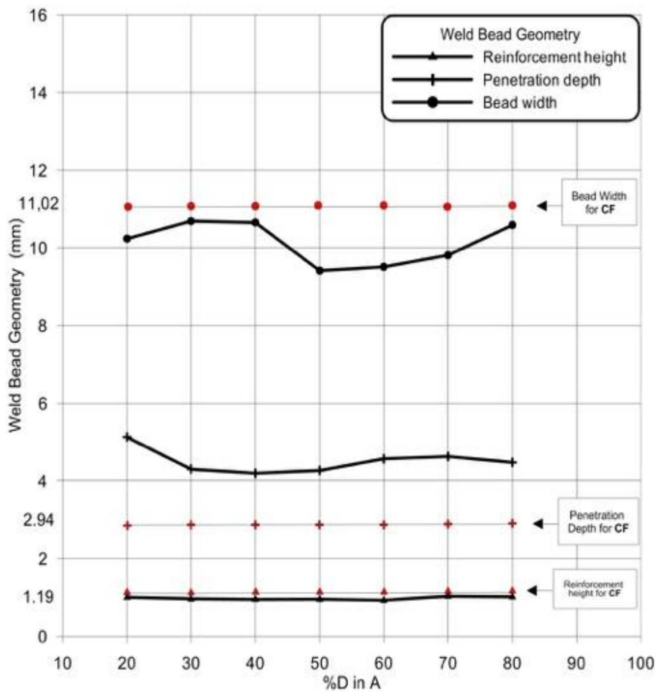

Figure 8. Effect of different A–D flux mixtures on weld bead geometry parameters
Note: Values are mean ± SD (n = 3).

For the mixtures with a low D content (20–40%), where the coarse particles of flux A were dominant, the weld bead width was relatively large. When the D content increased to 50–60%, the bead width decreased. A further increase in D to 70–80% resulted in a slight increase in bead width.

As shown in Figure 8, the penetration depth also changed with the D content, but the variation was not linear. It initially decreased and reached a minimum at about 40–50% D. A slight increase was then observed at 60–70% D, followed by another decrease at 80% D. These results show that the PSD of the binary flux mixture affects the weld bead geometry under the welding conditions used in this study.

The reinforcement height showed relatively small changes as the D content increased. Overall, the mixtures containing 50–60% D resulted in a relatively narrow bead width, sufficient penetration, and stable reinforcement height.

A coarse flux is more porous, which can lead to a more "open" arc and a wider molten pool, explaining the larger bead width. Conversely, a fine flux is more compact, improving arc confinement and heat transfer to the metal, which can increase penetration, as observed for flux D.

3.2 Microhardness results

Vickers microhardness tests were carried out on samples prepared from the SAW-welded plates. Measurements were taken at 1 mm intervals across the welded joint, and the results are presented in Figures 9–11. The results show that flux particle size has a noticeable effect on the hardness distribution across the welded joints.

Based on the metallographic observations, the HAZ width was approximately 1.8–2.5 mm, depending on the flux condition. The selected 1 mm spacing was considered adequate for identifying the general hardness trends across the welded joint; however, it limits the spatial resolution within the relatively narrow HAZ and may not capture localized hardness gradients in detail.

Figure 9 presents the microhardness profiles obtained using the CF and the four fluxes A, B, C, and D, with average particle sizes of 1.5, 0.75, 0.375, and 0.2 mm, respectively.

For fluxes A, B, C, and D, higher hardness values were observed in the WM, followed by a gradual decrease toward the HAZ and BM. The coarse flux A produced a relatively uniform hardness profile across the welded joint. In comparison, the finer fluxes C and D showed higher hardness values near the WM, together with more noticeable changes in hardness across the HAZ. Flux B showed an intermediate behavior between the coarse and fine fluxes.

These results indicate that the flux particle size affects the hardness distribution across the welded joint. The increase in microhardness observed with finer fluxes suggests higher cooling rates, which are likely to lead to harder microstructures (e.g., bainitic or martensitic constituents) compared to the softer microstructures (ferrite and pearlite) obtained with slower cooling rates. However, a detailed microstructural characterization by optical and electron microscopy is necessary to confirm these hypotheses.

Figure 10 shows the microhardness profiles obtained using the CF, fluxes A and D, and the binary mixtures AD20, AD50, and AD80.

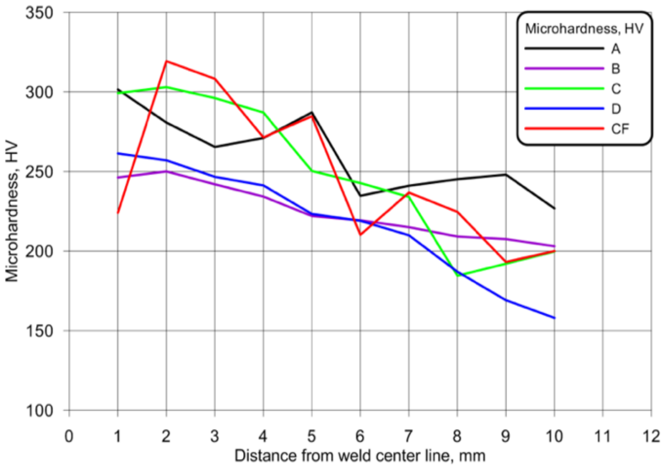

Figure 9. Microhardness profiles for commercial flux (CF) and the four fluxes A, B, C, and D

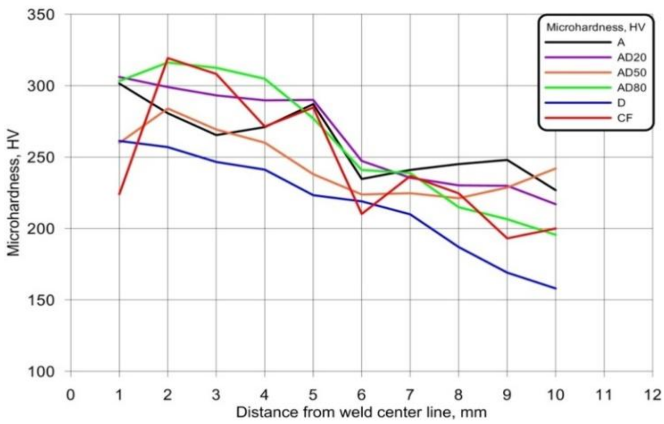

Figure 10. Microhardness profiles for commercial flux (CF), fluxes A and D, and the binary mixtures AD20, AD50 and AD80

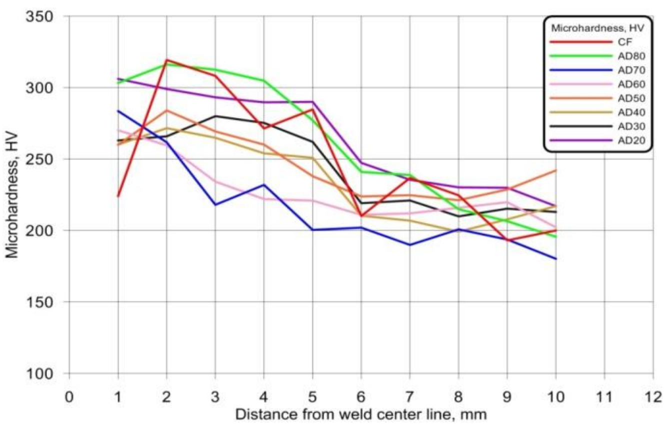

Figure 11. Microhardness profiles for commercial flux (CF) and the binary flux mixtures AD20, AD30, AD40, AD50, AD60, AD70, and AD80

The mixtures with a higher proportion of fine particles, particularly AD50 and AD80, exhibited higher microhardness values in the WM. These differences may be related to changes in the thermal conditions during welding associated with the PSD of the flux. The mixed fluxes also showed relatively uniform hardness profiles, with AD80 exhibiting a profile comparable to that of CF. These results highlight the influence of flux PSD on the microhardness of the welded joint.

Figure 11 shows the microhardness profiles obtained for the CF and the binary mixtures AD20, AD30, AD40, AD50, AD60, AD70, and AD80. The results show that the microhardness generally increased with increasing proportion of fine particles, especially in the WM and near the HAZ.

The AD80 weld, which contained the highest proportion of fine particles, showed the highest hardness values, reaching approximately 320 HV and exceeding those of the CF and all other mixtures. This increase may be related to changes in the thermal conditions during welding caused by the different PSDs of the flux mixtures. A finer flux, with better thermal insulation of the weld pool, could lead to slower cooling, potentially promoting the formation of acicular ferrite (good toughness). However, a very high fraction of fine particles, as in AD80, could lead to higher slag viscosity, trapping the arc and modifying heat transfer, which could explain the lower ductility observed. In comparison, AD20 and AD30, which contained lower proportions of fine particles, showed lower hardness values and more gradual changes across the welded joint. The mixtures from AD40 to AD60, particularly AD50, showed a more uniform hardness distribution across the weldment.

3.3 Tensile strength results

First, the effect of flux particle size on tensile properties was investigated using CF and four flux grades: A (1.5 mm), B (0.75 mm), C (0.375 mm), and D (0.2 mm), as shown in Figures 12 and 13.

The results shown in Figures 12 and 13 indicate that the mechanical behavior of the welded joints is influenced by flux particle size. Compared with CF, the coarse flux A showed lower tensile strength and ductility. The intermediate-grain-size fluxes B and C showed slightly lower tensile strength but maintained relatively good ductility. In contrast, the very fine flux D showed the highest UTS and ductility among the tested fluxes.

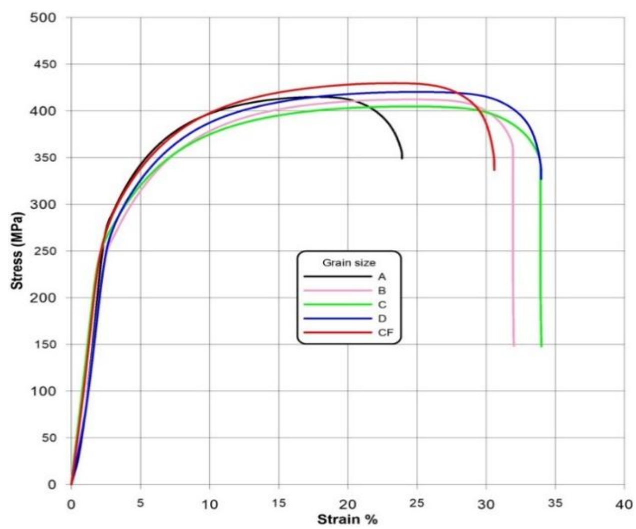

Figure 12. Stress–strain curves of welds produced using commercial flux (CF) and flux grades A, B, C, and D

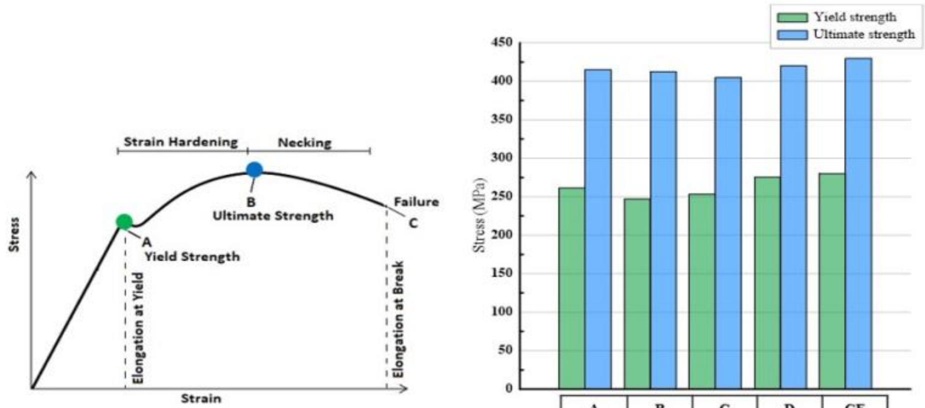

	A	B	C	D	CF
Yield strength	261.21 ± 2.56	247.17 ± 2.42	253.23 ±2.1	275.2 ±3.09	280.03 ±2.59
Ultimate strength	415.03 ± 3.53	412.24 ± 2.99	404.81 ± 3.84	420.27 ±3.01	429.7. ± 3.62

Figure 13. Tensile properties obtained from the stress–strain curves of welds produced using commercial flux (CF) and flux grades A, B, C, and D

Note: Values are mean ± SD (n = 3).

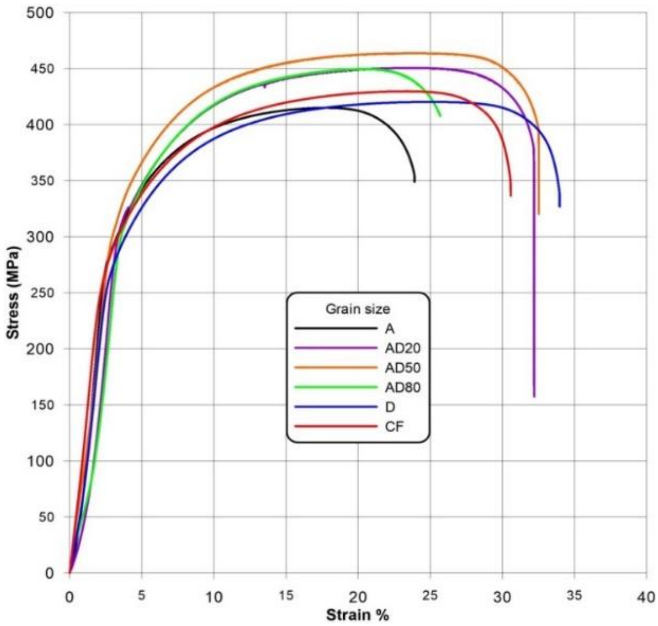

Figure 14. Stress–strain curves of welds produced using commercial flux (CF), flux grades A and D, and the A–D mixtures AD20, AD50, and AD80

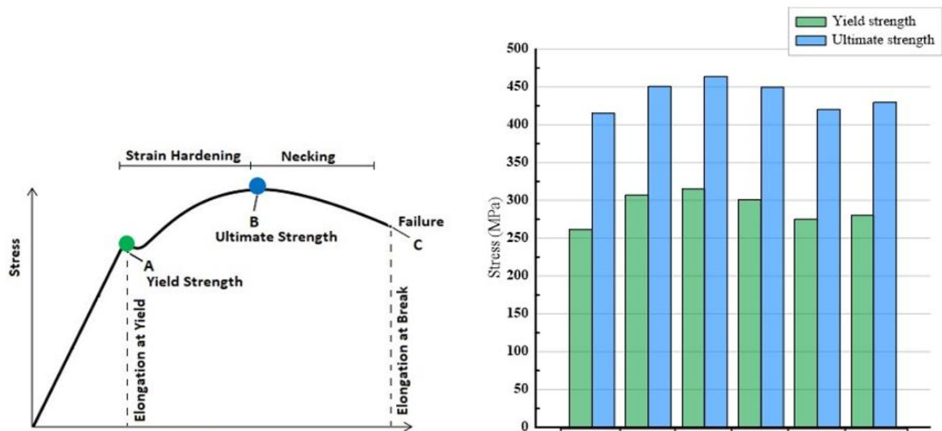

	A	AD20	AD50	AD80	D	CF
Yield strength	261.21 ± 2.56	307.11 ± 3.89	315,2 ± 3.32	300.9 ± 4.25	275.2 ±3.09	280.03 ± 2.59
Ultimate strength	415.03 ± 3.53	450.5 ± 4.72	463.8. ± 3.51	449.6 ± 5.04	420.27 ± 3.01	429.7 ± 3.62

Figure 15. Tensile properties obtained from the stress–strain curves of welds produced using commercial flux (CF), flux grades A and D, and the A–D mixtures AD20, AD50, and AD80

Note: Values are mean ± SD (n = 3).

As illustrated in Figures 14 and 15, the tensile properties of the single-particle-size fluxes and CF are compared with those of the AD20, AD50, and AD80 mixtures. The AD50 mixture exhibited a relatively wide plastic region and high UTS, indicating a favorable strength–ductility balance. AD80 showed high tensile strength but lower ductility, while AD20 also exhibited good tensile behavior, although slightly lower than that of AD50.

Finally, Figures 16 and 17 present the stress–strain curves obtained for the different A-D mixtures, including AD20, AD30, AD40, AD50, AD60, AD70, and AD80, together with CF.

Figure 16 shows that the mechanical behavior of the SAW joints is influenced by the flux PSD. Mixtures with a low fine-particle content (AD20–AD30) showed a gradual increase in tensile strength and elongation. Intermediate mixtures (AD50–AD70) exhibited higher UTS and a relatively extended plastic deformation range, indicating a favorable strength–ductility balance. Among the tested mixtures, AD50 showed the most favorable overall tensile response. However, a further increase in fine-particle content, as in AD80, resulted in lower ductility, suggesting that excessive fine-particle content may adversely affect the tensile performance of the welded joints.

Intermediate mixtures exhibited stress–strain curves consistent with ductile fracture behavior; however, this interpretation remains to be validated by fractographic examination.

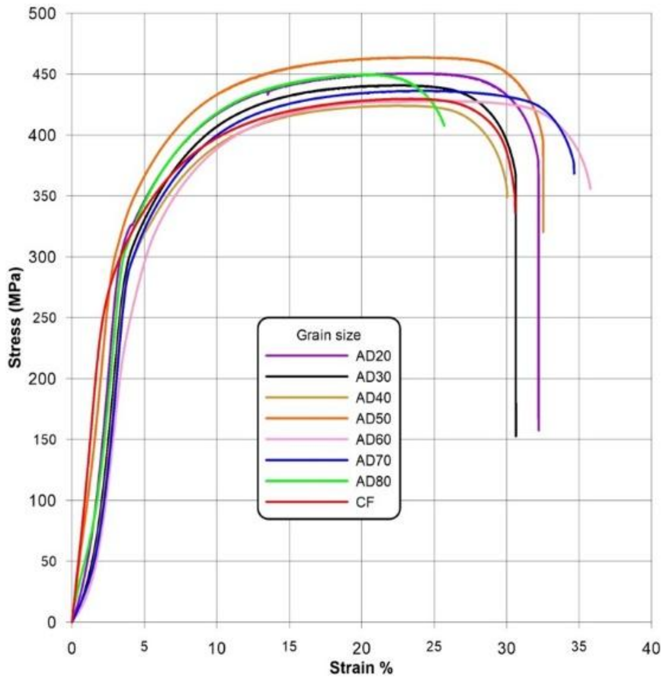

Figure 16. Stress-strain curves of welds produced using CF and the A–D mixtures AD20, AD30, AD40, AD50, AD60, AD70, and AD80

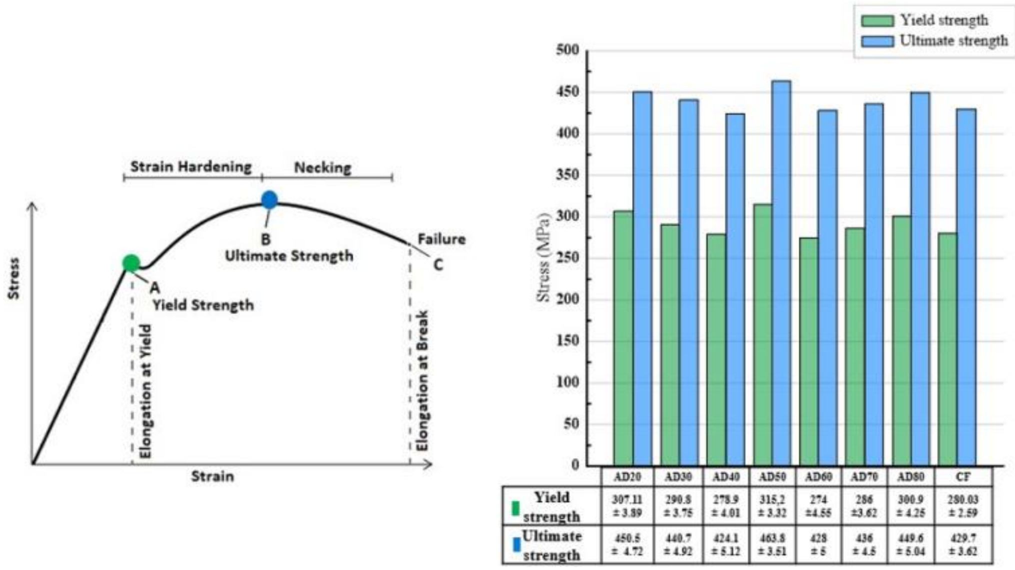

Figure 17. Tensile properties obtained from the stress–strain curves of welds produced using CF and the A–D mixtures AD20, AD30, AD40, AD50, AD60, AD70, and AD80

Note: Values are mean ± SD (n = 3). Commercial flux (CF).

4. CONCLUSIONS

An experimental investigation was conducted to evaluate the effects of flux particle size and mixed PSD on weld bead geometry and mechanical properties during SAW of low-carbon steel used for LPG cylinder applications. The main findings can be summarized as follows:

•Compared with CF, the use of flux grades A, B, C, and D generally resulted in increased bead width and penetration depth. The largest increase in bead width was observed for flux B, while the highest penetration depth was obtained with flux D. A slight reduction in reinforcement height was also observed, particularly for flux D.

•Mixtures containing approximately 50–60% fine-grained flux D provided favorable weld bead geometry, characterized by a relatively narrow bead width, adequate penetration, and stable reinforcement height.

•Increasing the proportion of fine-grained flux D in the A-D mixtures generally resulted in higher microhardness values, particularly in the WM and near the HAZ.

•Welds produced with lower fractions of fine particles, such as AD20 and AD30, showed lower hardness values and more gradual variations across the welded joint.

•Intermediate mixtures, from AD40 to AD60, showed a relatively uniform hardness distribution across the welded joint, with AD50 showing a particularly uniform profile.

•Overall, among the tested mixtures (20–80 wt.% D), the AD50 mixture (50% D–50% A) exhibited the highest UTS and a relatively extended plastic deformation range, indicating a favorable balance between strength and ductility, while also providing the most favorable combination of weld bead geometry, tensile properties, and hardness distribution.

•The CF exhibited intermediate tensile properties compared with the investigated flux conditions, which may be related to its broad particle size range, although its detailed PSD was not quantitatively characterized.

It should be noted that the PSD of the CF was not quantitatively characterized in this study, and this constitutes a limitation of the present work. Future work will include detailed metallographic analyses using optical microscopy, SEM, and EBSD to investigate and validate the microstructural mechanisms associated with the observed hardness variations. In addition, measurements of arc voltage and gas pressure will be performed to directly assess arc stability and further support the interpretations presented in this study.

ACKNOWLEDGMENT

The authors would like to acknowledge the support and assistance provided by the institutions and individuals who contributed to the completion of this work.

REFERENCES

[1] Tripathi, A., Kumar, A., Chandrakar, M.K. (2017). Design and analysis of a composite cylinder for the storage of liquefied gases. International Journal for Scientific Research & Development, 5(3): 871-876.

[2] Bandhavi, C., Rao, N.A.N. (2012). Design and analysis of LPG cylinder using ANSYS software. International Journal of Mathematical Sciences, Technology and Humanities, 58(4): 635-646.

[3] Kumar, V. (2011). Development and characterization of fluxes for submerged arc welding. Shodhganga. Ph.D. dissertation, Punjabi University, India. https://shodhganga.inflibnet.ac.in/handle/10603/2065.

[4] McPherson, N.A., Chi, K., Baker, T.N. (2003). Submerged arc welding of stainless steel and the challenge from the laser welding process. Journal of Materials Processing Technology, 134(2): 174-179. https://doi.org/10.1016/S0924-0136(02)00466-1

[5] Paniagua-Mercado, A.M., López-Hirata, V.M., Saucedo-Muñoz, M.L. (2025). Influence of the chemical composition of flux on the microstructure and tensile properties of submerged-arc welds. Journal of Materials Processing Technology, 169(3): 346-351. https://doi.org/10.1016/j.jmatprotec.2005.03.035

[6] Olson, D.L., Siewert, T.A., Liu, S., Edwards, G.R. (1993). Procedure development and practice considerations for electron-beam welding. In ASM Handbook: Welding, Brazing, and Soldering. ASM International, pp. 851-873. https://doi.org/10.31399/asm.hb.v06.a0001444

[7] Li, K., Wu, Z.S., Liu, C.R., Chen, F.H. (2014). Arc characteristics of submerged arc welding with stainless steel wire. International Journal of Minerals, Metallurgy and Materials, 21(8): 772-778. https://doi.org/10.1007/s12613-014-0970-1

[8] Correia, D.S., Ferraresi, V.A. (2007). Welding process selection through a double criterion: Operational costs and non-quality costs. Journal of Materials Processing Technology, 184(1-3): 47-55. https://doi.org/10.1016/j.jmatprotec.2006.11.006

[9] Gupta, D., Bansal, A., Jindal, S. (2024). Effect of fluxes in submerged arc welding for steel: A review. Materials Today: Proceedings. https://doi.org/10.1016/j.matpr.2024.05.053

[10] Houldcroft, P.T. (1990). Submerged-Arc Welding. Woodhead Publishing, Cambridge. https://doi.org/10.1016/C2013-0-17447-8

[11] Davis, L. (1981). An Introduction to Welding Fluxes for Mild and Low Alloy Steels. Welding Institute, Cambridge.

[12] Kanjilal, P., Pal, T.K., Majumdar, S.K. (2006). Combined effect of flux and welding parameters on chemical composition and mechanical properties of submerged arc weld metal. Journal of Materials Processing Technology, 171(2): 223-231. https://doi.org/10.1016/j.jmatprotec.2005.06.083

[13] Murugan, N., Gunaraj, V. (2005). Prediction and control of weld bead geometry and shape relationships in submerged arc welding of pipes. Journal of Materials Processing Technology, 168(3): 478-487. https://doi.org/10.1016/j.jmatprotec.2005.03.001

[14] Pandey, N.D., Bharti, A., Gupta, S.R. (1994). Effect of submerged arc welding parameters and fluxes on element transfer behaviour and weld-metal chemistry. Journal of Materials Processing Technology, 40(1-2): 195-211. https://doi.org/10.1016/0924-0136(94)90486-3

[15] Zhang, J., Xu, Q. (2022). Probing element transfer behavior during the submerged arc welding process for CaF2-SiO2-Na2O-Cr2O3 agglomerated fluxes: A thermodynamic approach. Processes, 10(10): 1900. https://doi.org/10.3390/pr10101900

[16] Patchett, B.M. (1983). Some effects of flux physical properties on weld-bead formation, in the SAW process. Journal of Materials for Energy Systems, 5: 165-175. https://doi.org/10.1007/BF02833370

[17] Singh, B., Khan, Z.A., Siddiquee, A.N. (2013). Effect of flux composition on element transfer during submerged arc welding (SAW): A literature review. International Journal of Current Research, 5(12): 4181-4186. https://www.journalcra.com/sites/default/files/issue-pdf/Download%204377.pdf.

[18] Burck, P.A., Indacochea, J.E., Olson, D.L. (1990). Effects of welding flux additions on 4340 steel weld metal composition. Welding Journal, 69(3): 115-122. https://scispace.com/papers/effects-of-welding-flux-additions-on-4340-steel-weld-metal-4iuqicdv2u.

[19] Coetsee, T., Mostert, R.J., Pistorius, P.G.H., Pistorius, P.C. (2021). The effect of flux chemistry on element transfer in submerged arc welding: Application of thermochemical modelling. Journal of Materials Research and Technology, 11: 2021-2036. https://doi.org/10.1016/j.jmrt.2021.02.046

[20] Park, J.Y., Chang, W.S., Sohn, I. (2012). Effect of MnO to hydrogen dissolution in CaF2-CaO-SiO2 based welding type fluxes. Science and Technology of Welding and Joining, 17(2): 134-140.

https://doi.org/10.1179/1362171811Y.0000000084

[21] Zhang, J., Coetsee, T., Basu, S., Wang, C. (2020). Impact of gas formation on the transfer of Ti and O from TiO2-bearing basic-fluoride fluxes to submerged arc welded metals: A thermodynamic approach. Calphad, 71: 102195. https://doi.org/10.1016/j.calphad.2020.102195

[22] Vishnu, B.R., Sivapirakasam, S.P., Satpathy, K.K., Albert, S.K., Chakraborty, G. (2018). Influence of nano-sized flux materials in the reduction of the Cr(VI) in the stainless steel welding fumes. Journal of Manufacturing Processes, 34: 713-720. https://doi.org/10.1016/j.jmapro.2018.07.009

[23] Garg, J., Garg, S.B., Jeet, B., Singh, H. (2022). The effects of flux particle size and column height on the bead geometry in submerged arc welding. Sādhanā, 47(4): 199. https://doi.org/10.1007/s12046-022-01971-7

[24] Siewert, T.A., Franke, G.L. (1990). Analysis and characterization of commercial welding fluxes. Welding Research Supplement, 69(7): 247s-255s. https://s3.us-east-1.amazonaws.com/WJ-www.aws.org/supplement/WJ_1990_07_s247.pdf.

[25] Mathers, G. (2020). Job knowledge 87: Submerged arc welding consumables. The Welding Institute. https://www.twi-global.com/technical-knowledge/job-knowledge/submerged-arc-welding-consumables-part-1-087.

[26] Patel, N. (2020). Submerged arc welding fluxes: The criticality of particle size. Welding Advisers. https://www.welding-advisers.com/submerged-arc-welding-fluxes-the-criticality-of-particle-size1.html.

[27] ASTM A36/A36M-19. (2019). Standard Specification for Carbon Structural Steel. ASTM International. https://doi.org/10.1520/A0036_A0036M-19

[28] ASME SFA-5.17. (2025). Specification for Carbon Steel Electrodes and Fluxes for Submerged Arc Welding. ASME Boiler and Pressure Vessel Code, Section II, Part C. American Society of Mechanical Engineers, New York. https://pubs.aws.org/p/2267/a517a517m2025-specification-for-carbon-steel-electrodes-and-fluxes-for-submerged-arc.

[29] ISO 14174:2019. (2019). Welding Consumables — Fluxes for Submerged Arc Welding and Electroslag Welding — Classification. International Organization for Standardization. https://www.iso.org/standard/73877.html.

[30] ASTM A370. (2024). Standard Test Methods and Definitions for Mechanical Testing of Steel Products. ASTM International. https://doi.org/10.1520/A0370-24

[31] ISO 9015-2. (2016). Destructive Tests on Welds in Metallic Materials – Hardness Testing – Part 2: Microhardness Testing of Welded Joints. Slovak Office of Standards, Metrology and Testing, Bratislava, Slovakia.

[32] Om, H., Pandey, S. (2013). Effect of heat input on dilution and heat-affected zone in submerged arc welding process. Sādhanā, 38(6): 1369-1391. https://doi.org/10.1007/s12046-013-0182-9

[33] Sarkar, A., Dey, P., Rai, R.N., Saha, S.C. (2016). A comparative study of multiple regression analysis and back propagation neural network approaches on plain carbon steel in submerged-arc welding. Sādhanā, 41(5): 549-559. https://doi.org/10.1007/s12046-016-0494-7

NOMENCLATURE

A	coarse: 1.0–2.0 mm
B	medium: 0.5–1.0 mm
C	fine: 0.25–0.5 mm
D	Very fine: 0.15–0.25 mm
CF	Commercial flux

Bead profile

H	Reinforcement height mm
P	Penetration depth mm
W	Bead width mm

Binary mixtures of A with D

AD20	20% D + 80% A
AD30	30% D + 70% A
AD40	40% D + 60% A
AD50	50% D + 50% A
AD60	60% D + 40% A
AD70	70% D + 30% A
AD80	80% D + 20% A

Welded zones

BM	Base metal
HAZ	Heat-affected zone
WM	Weld metal